

Electronic Supplementary Information (ESI)

An iron-nitrogen doped carbon and CdS hybrid catalytic system for efficient CO₂ photochemical reduction

*Jin-Han Guo, Xiao-Yao Dao and Wei-Yin Sun**

Coordination Chemistry Institute, State Key Laboratory of Coordination Chemistry, School of Chemistry and Chemical Engineering, Nanjing National Laboratory of Microstructures, Collaborative Innovation Center of Advanced Microstructures, Nanjing University, Nanjing 210023, China

* Corresponding author.

E-mail address: sunwy@nju.edu.cn.

Characterization

Powder X-ray diffraction (PXRD) data were collected on a Bruker D8 Advance X-ray diffractometer with Cu K α ($\lambda = 1.5418 \text{ \AA}$) radiation. The gas adsorption isotherms were measured on a Micromeritics ASAP 2020 system by employing a standard volumetric technique up to saturated pressure. Before gas adsorption experiments, the sample was activated under a dynamic vacuum at 200 °C for 6 hours. The N₂ adsorption isotherms were monitored at 77 K. The X-ray photoelectron spectroscopy (XPS) measurements were conducted by using an ESCALAB 250XI high-performance electron spectrometer using monochromated Al K α radiation ($h\nu = 1486.7 \text{ eV}$) as the excitation source. The XPS data were analyzed by the XPSPEAK41 software package. The total content of Fe was quantified by an Agilent 7700X ICP-MS. Scanning electron microscope (SEM) observations were performed on a Hitachi S-4800 field emission scanning electron microscope at an accelerating voltage of 5 kV. UV-Vis diffuse reflectance spectra (DRS) were recorded on a Shimadzu UV-3600 spectrophotometer

in the wavelength range of 200-800 nm (BaSO_4 purchased from Sigma-Aldrich was used as reference). ^1H NMR spectra were collected on a 500 MHz Bruker Advance DRX NMR instrument at room temperature with water peak suppressed. The $^{13}\text{CO}_2$ isotopic labeling was conducted by a GC-MS (Trace GC Ultra).

Preparation of the materials

Fe-CB was prepared following the previous report with minor modifications.¹ Different weight of TPPFeCl (Energy Chemical) was mixed with 200 mg CB (Cabot XC-72r) in 50 ml dichloromethane. Then sonicating the mixture for 30 min to form a uniform suspension. Dichloromethane was evaporated to form the precursor of the catalyst. The precursors were heated to 800 °C in a N_2 flow with a heating rate of 5 °C min^{-1} , then maintained at 800 °C for 2 hours to yield a black powder. The powder was washed with 1 M HCl aqueous solution at 70 °C for 6 h to remove formed iron particles and washed with water several times then dried under vacuum.

The preparation of Ni-CB is performed according to our previous report.¹

The preparation of CdS is according to the previous reports.^{2,3} 100 mg of cadmium acetate was dissolved in 10 ml of dimethyl sulfoxide (DMSO) under sonication. Then, the formed solution was transferred into a 20 ml Teflon-lined autoclave and was heated at 180 °C for 12 h. After natural cooling, the luminous yellow precipitate was separated by centrifugation. Then the solid was washed by acetone twice and ethanol twice to remove superfluous DMSO, and dried at 120 °C overnight under the vacuum.

Electrochemical tests

The polarization curves and the electrochemical impedance spectroscopy (EIS) of the catalysts were measured in a commercial H-cell (Gaoss Union) using a carbon paper (TGP-H-

060, Toray) with an electroactive area of 1 cm² coated with 0.5 mg cm⁻² catalysts. A Nafion 117 membrane was used to separate the cell. A saturated Ag/AgCl electrode was used as a reference and a Pt plate was used as the counter electrode. An electrochemical workstation (CHI 730E) was employed for polarization curve tests. The Ohmic drops between the working and the reference electrodes were 90% compensated by the electrochemical workstation. Electrode potentials were rescaled to SHE reference by $E_{SHE} = E_{Ag/AgCl} + 0.197$ V. CO₂ was purged into 0.5 M KHCO₃ aqueous solution for 30 min to prepare a CO₂-saturated electrolyte (pH = 7.3), the gas flow was kept at 20 ml min⁻¹ using a mass flow controller (MFC, MFC300, Aitolys) during the measurements, the MFC was calibrated by a soap-film flowmeter that calibrated by an analytical balance (ME204E /02, Mettler Toledo). A Zahner IM6ex workstation was utilized in EIS tests, the measurements were performed with a bias potential of -0.9 V vs. SHE with a frequency range from 10⁻¹ to 10⁵ Hz. The onset potential for CO is the lowest potentials at which the GC detector signal of the CO is at least 5 times higher than the noise signal.

Photocurrent measurements were recorded on the CHI 730E electrochemical workstation in a standard three-electrode system with a photocatalyst-coated ITO as working electrode, a Pt plate as the counter electrode and a Ag/AgCl as the reference electrode. An aqueous solution of 10 wt% TEOA and 0.5 M KHCO₃ saturated with CO₂ was used as the electrolyte (pH = 8.8). The catalytic ink was prepared by adding 10 mg CdS or 1 mg Fe-CB or the mixture of them into 1.0 mL of 2.5 ‰ Nafion (Du Pont) ethanol solution, and the working electrode was prepared by dropping the suspension (100 μL) onto an ITO glass on a heating plate with an active area of 1 cm². The photocurrent signals of the samples were measured under chopped light at 0.3 V vs. SHE.

The Mott-Schottky test was performed on the Zahner electrochemical workstation in a standard three-electrode system with a CdS-coated glassy carbon as working electrode, a Pt wire as the counter electrode and a Ag/AgCl as the reference electrode. A 0.5 M Na₂SO₄ solution was used as the electrolyte. The working electrode was prepared by dropping the CdS ink onto the surface of glassy carbon and dried under an infrared lamp to form a tight-packed layer. The measurements were carried out under frequencies of 1, 1.5, and 2 kHz.

Photochemical tests

The photochemical tests were performed in a batch-type reaction system (CEL-SPH2N-D9, CeAulight) equipped with a 50 ml photoreactor together with a quartz plate as the cap. Firstly, 1 mg of catalysts and 10 mg of CdS were suspended in 25 ml of 10 wt% triethanolamine (TEOA) and 0.5 M KHCO₃ aqueous solution. The suspensions were sonicated for 30 min to give dark green turbid liquids. Ultra-pure CO₂ (99.999%) was purged into the liquids for 30 min for saturation. Then the mixtures were transferred into the photoreactor and the reactor was held at 25 °C using circulating water. After the evacuation of the reaction system (no O₂ or N₂ could be detected), pure CO₂ gas was injected into the closed system until the pressure maintained at 80 kPa. A 300 W xenon arc lamp (Sirius-300P, Zolix Instruments Co., Ltd.) with an AM 1.5G filter (CeAulight) was used as the light source. The optical power densities were set to ~400 mW cm⁻² calibrated by an optical power meter (CEL-NP2000-2, CeAulight). The gas products were detected by gas chromatography (GC-9860, Luchuang Instrument), equipped with a TCD detector and an FID detector. A 1 m TDX-01 column with N₂ (99.999%) as the carrier gas was utilized for gas separation, the temperatures for TCD and FID were set to 100 and 150 °C, respectively. The retention times of CO and H₂ are 1.38, and 0.71 min, respectively.

The turnover number (TON) of the catalysts were calculated based on following equation:

$$TON = \frac{Y_{CO} \times M_{metal}}{m_{cat} \times w_{icp}}$$

In the equation, Y_{CO} is yield of CO (mol), M_{metal} is the molecular weight of the metal (g mol^{-1}), m_{cat} is the weight of catalyst utilized in the photocatalysis (g), w_{icp} is the weight percentage of metal in the catalysts (%). As for the Fe-CB+CdS system, Y_{CO} is 111×10^{-6} mol, M_{metal} is 56 g mol^{-1} , m_{cat} is 0.001 g, and w_{icp} is 0.51%, thus, we have the TON of Fe-CB is 1.22×10^3 . For Ni-CB+CdS, Y_{CO} is 9.5×10^{-6} mol, M_{metal} is 59 g mol^{-1} , m_{cat} is 0.001 g, and w_{icp} is 0.58%, thus, we have the TON of Ni-CB is 97.

DFT simulation

According to previous reports, pyrolyzing TPPM molecule leads to the formation of the M-N₄ coordination structure,⁴⁻⁶ thus, we utilized the M-N₄ structure on the graphene sheet to simulate the catalysts in the DFT calculation.

Vienna ab initio simulation package (VASP)⁷ was used to perform all the density functional theory (DFT) computations. The projector augmented wave (PAW)⁸ pseudopotential was used for the core electrons and a 480 eV cutoff energy for the valence electrons. The generalized gradient approximation (GGA) in the form of Perdew-Burke-Ernzerhof (PBE)⁹ was employed for the exchange-correlation potentials.

The M-N-C catalysts were simulated using a (6 × 6) graphene sheet with metal bonding to four N atoms in a double vacancy of graphene. Vacuum spaces of ~10 Å along the Z-direction were used. A 3 × 3 × 1 Γ -centered k-mesh was used to sample the first Brillouin-zone with Gaussian smearing. The self-consistent field (SCF) convergence criterion was set to 1×10^{-5}

eV for electronic iteration and the ionic relaxation continued until the maximum force less than 0.02 eV Å⁻¹.

The Gibbs free energies (G) were calculated at 298 K and 1 atm as outlined below:

$$G = E_{DFT} + E_{ZPE} + \int_0^{298} C_V dT - T\Delta S$$

where E_{DFT} , E_{ZPE} , C_V , and S represent the energy calculated by DFT, the vibrational zero-point energy, the heat capacity at constant volume, and the entropy, respectively.

Gas-phase molecules were treated using the ideal gas approximation, the adsorbates were treated using a harmonic approximation. The DFT-calculated energy for CO₂ was corrected by +0.45 eV to correct the overestimation by DFT.^{10, 11} The relative free energies were calculated based on the computational hydrogen electrode (CHE) model.^{11, 12}

Crystal orbital Hamilton population (COHP) analysis was processed by the LOBSTER 4.0.0 software package based on the DFT results.¹³⁻¹⁵ According to the COHP analysis, we can determine the contribution of bonding between the neighboring atoms, and the bond strengths can be estimated by integrating the COHP under the Fermi level of the optimized structures.

Supplementary Note:

As for the origination of hydrogen, we perform a simple calculation as follow:

Since the pK_a of the hydroxy group in TEOA is ~ 14.2 , we have:

$$\frac{[\text{TEOA}^-][\text{H}^+]}{[\text{TEOA}]} = 10^{-14.2},$$

$$\text{And } [\text{OH}^-][\text{H}^+] = 10^{-14},$$

Thus, we have:

$$\frac{[\text{TEOA}^-]}{[\text{TEOA}][\text{OH}^-]} = 0.63,$$

and $[\text{TEOA}]$ is ~ 0.7 M in our system, thus, we have:

$$\frac{[\text{TEOA}^-]}{[\text{OH}^-]} = 0.9,$$

Thus, we have the ionization amount of TEOA and H_2O in the same order of magnitudes.

Also, due to the proton exchange between TEOA and water, we consider that the hydrogen is originated from both water and TEOA in our system. Also, in our previous report, we performed a labelling experiment to verify this point (*Chemical Science*, 2019, **10**, 4834–4838).

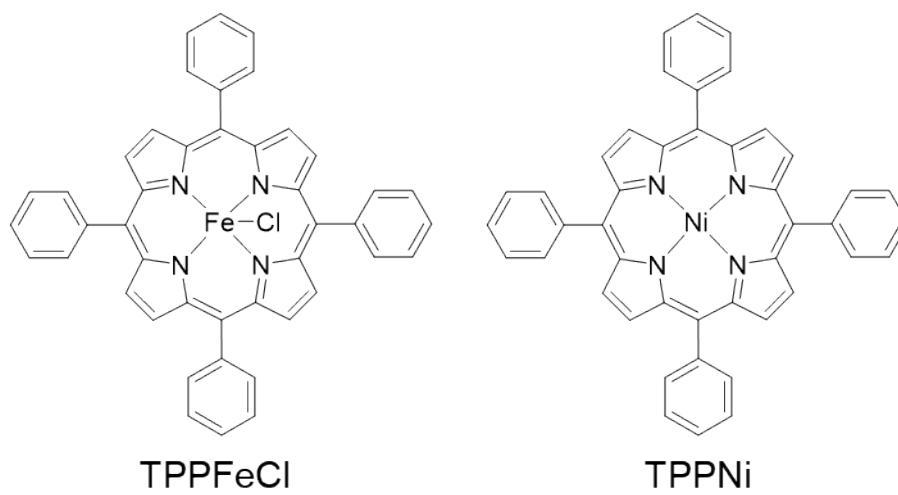


Fig. S1 Chemical structures of TPPFeCl and TPPNi.

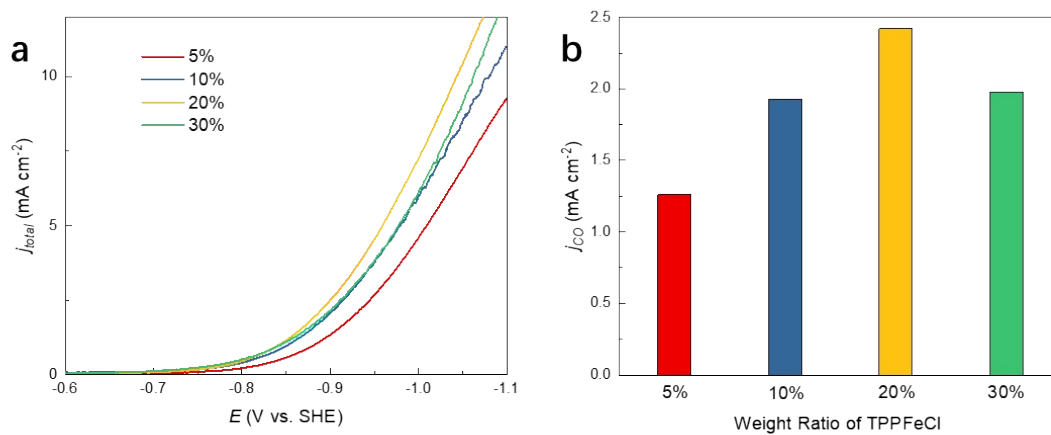


Fig. S2 (a) LSV curves of Fe-CB with the different weight ratios of TPPFeCl in the precursors in CO_2 saturated 0.5 M KHCO_3 aqueous solution; (b) CO partial current densities on different Fe-CB catalysts.

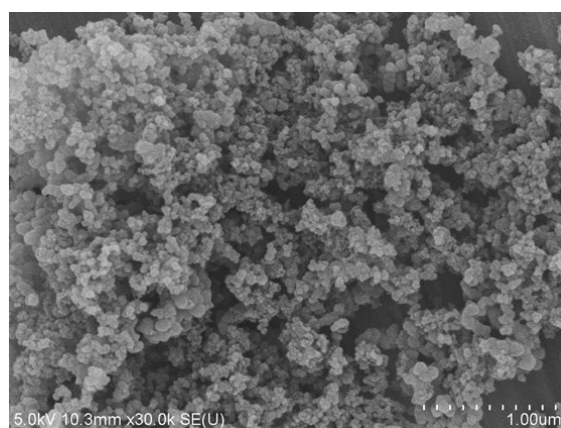
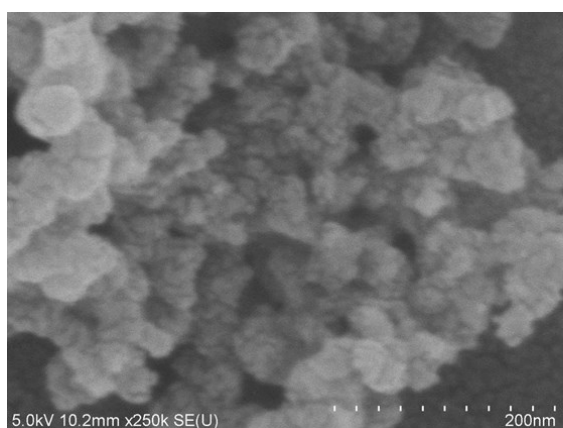


Fig. S3 SEM images of Fe-CB showing the rough surface (left) and the 3D porous structure (right).

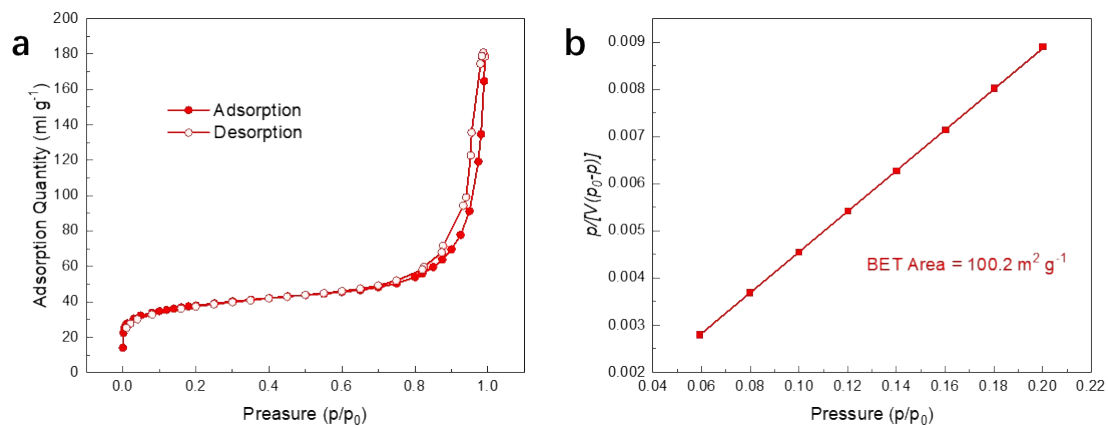


Fig. S4 N₂ adsorption measurement of Fe-CB. (a) N₂ adsorption isotherms at 77 K. (b) BET analysis.

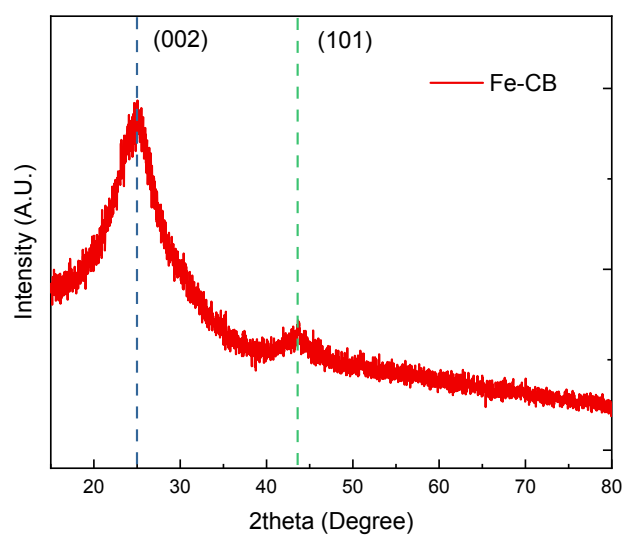


Fig. S5 PXRd pattern of Fe-CB, only graphite (002) and (101) diffraction patterns were detected.

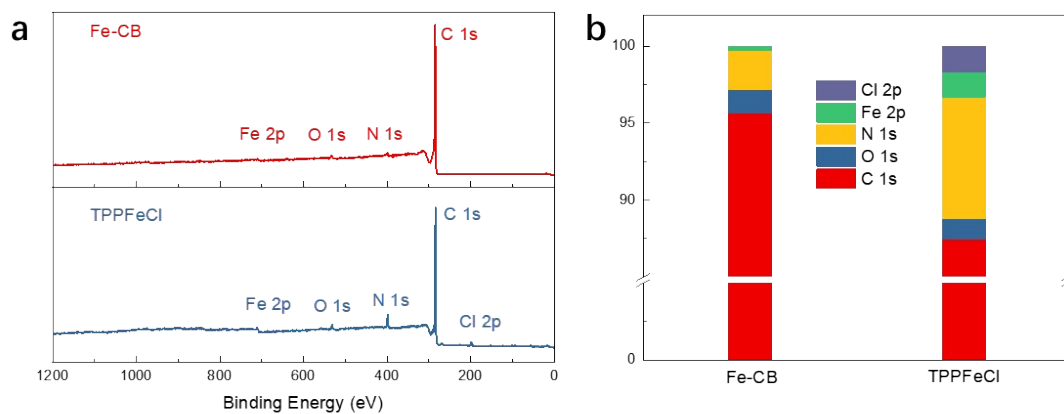


Fig. S6 XPS survey of Fe-CB and TPPFeCl. (a) XPS survey spectra of Fe-CB and TPPFeCl, only Ni, N, C, Cl, and O elements were detected. (b) The atomic percentage of the elements in Fe-CB and TPPFeCl.

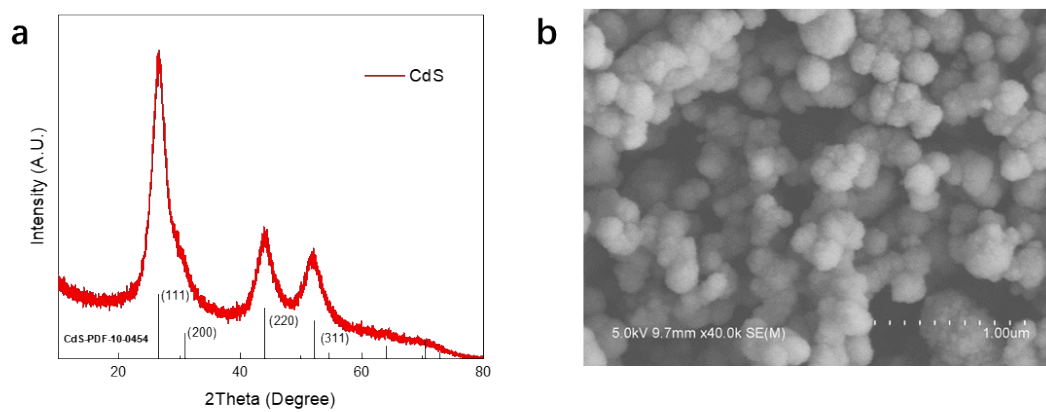


Fig. S7 (a) PXRD pattern of CdS. (b) SEM image of CdS.

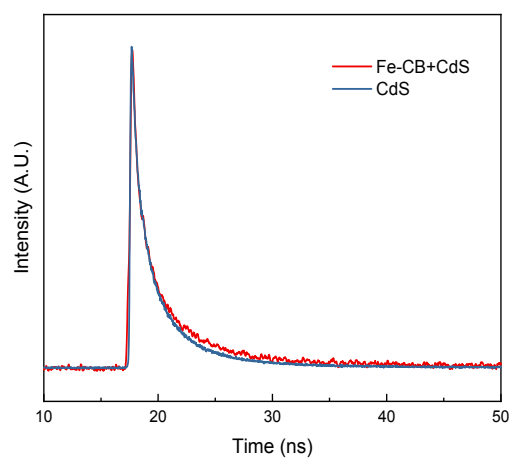


Fig. S8 Time-resolved PL decay spectra of Fe-CB+CdS and CdS samples.

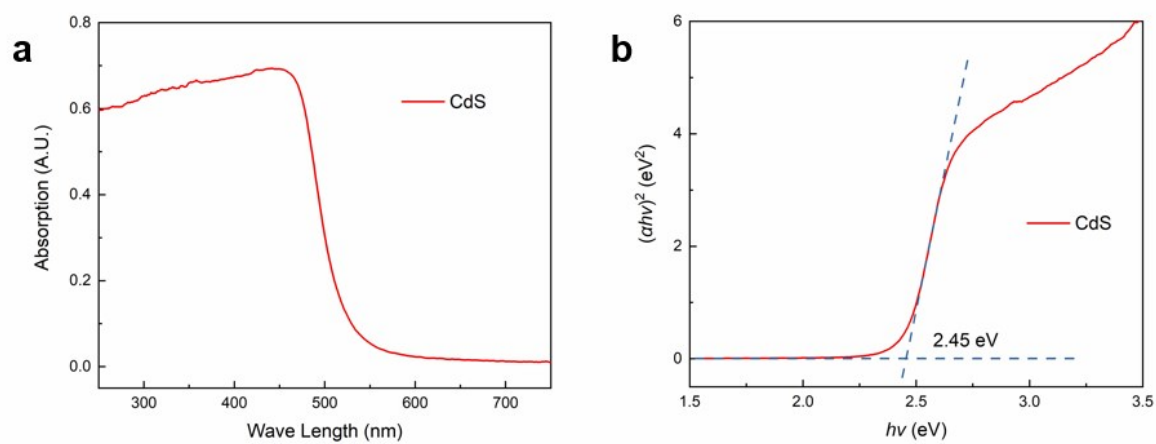


Fig. S9 (a) UV-vis-DRS spectrum of CdS. (b) Tauc-plot of CdS.

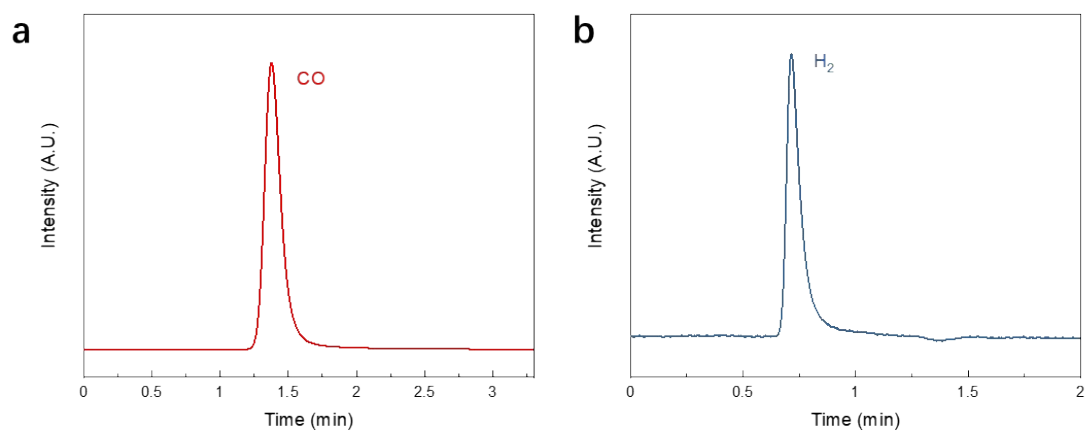


Fig. S10 The gaseous products upon solar-light irradiation analyzed by GC. (a) CO signal detected on the FID detector with a retention time of 1.38 min, (b) H₂ signal detected on the TCD detector with a retention time of 0.71 min.

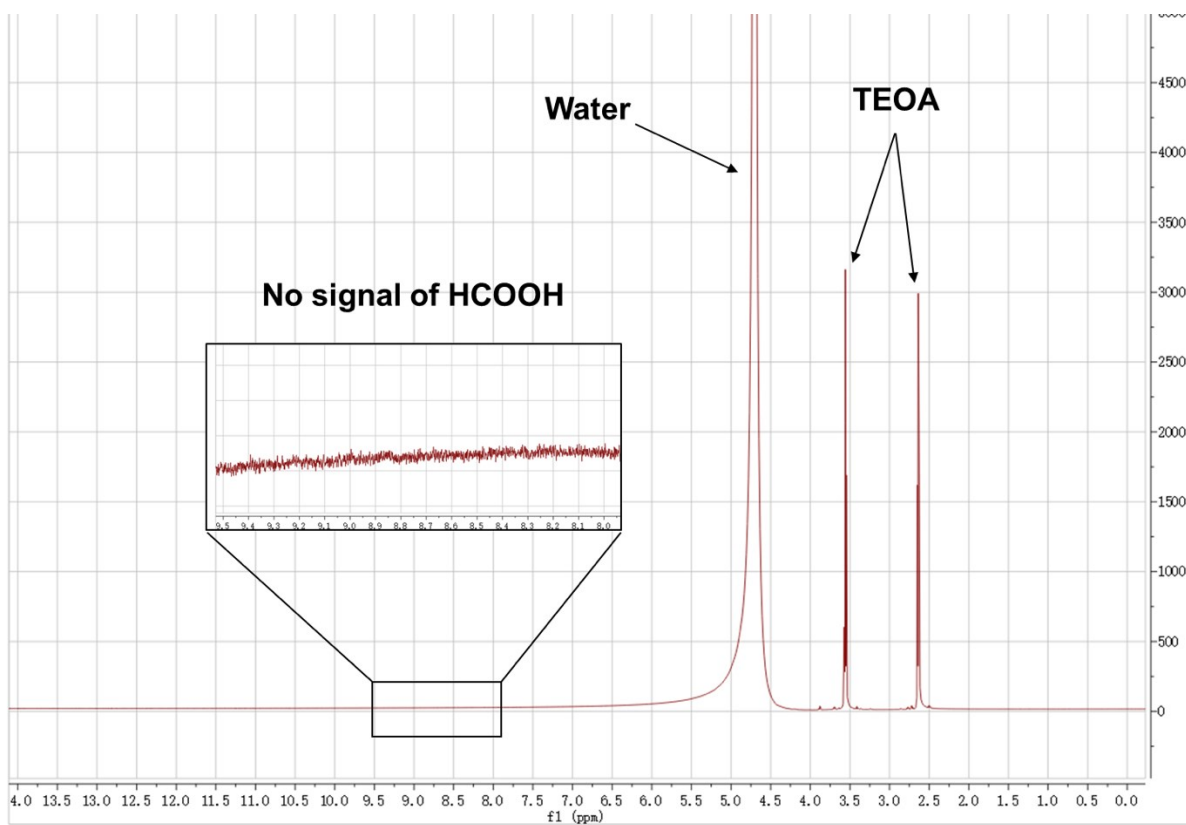


Fig. S11 ^1H NMR spectrum of the solution after 8 h of photocatalysis.

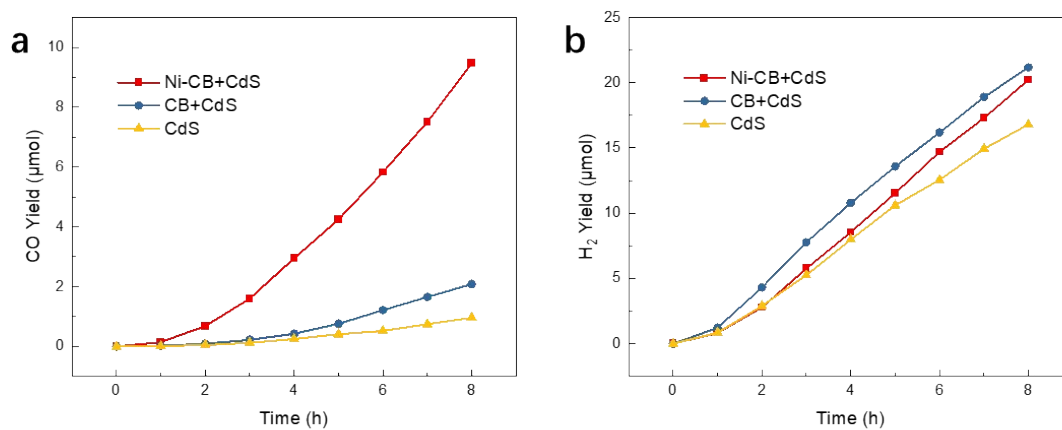


Fig. S12 Photochemical CO (a) and H₂ (b) production as a function of time of the hybrid systems.

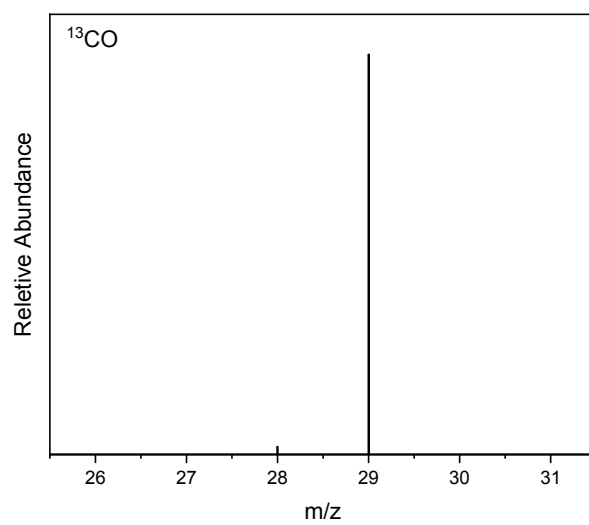


Fig. S13 Mass spectrum of ^{13}CO generated from the photoreduction of $^{13}\text{CO}_2$ isotopic experiment.

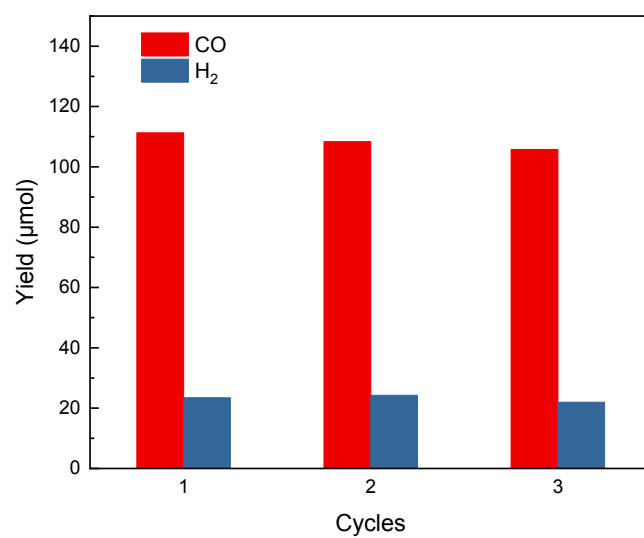


Fig. S14 CO and H₂ yields of Fe-CB for successive three cycles.

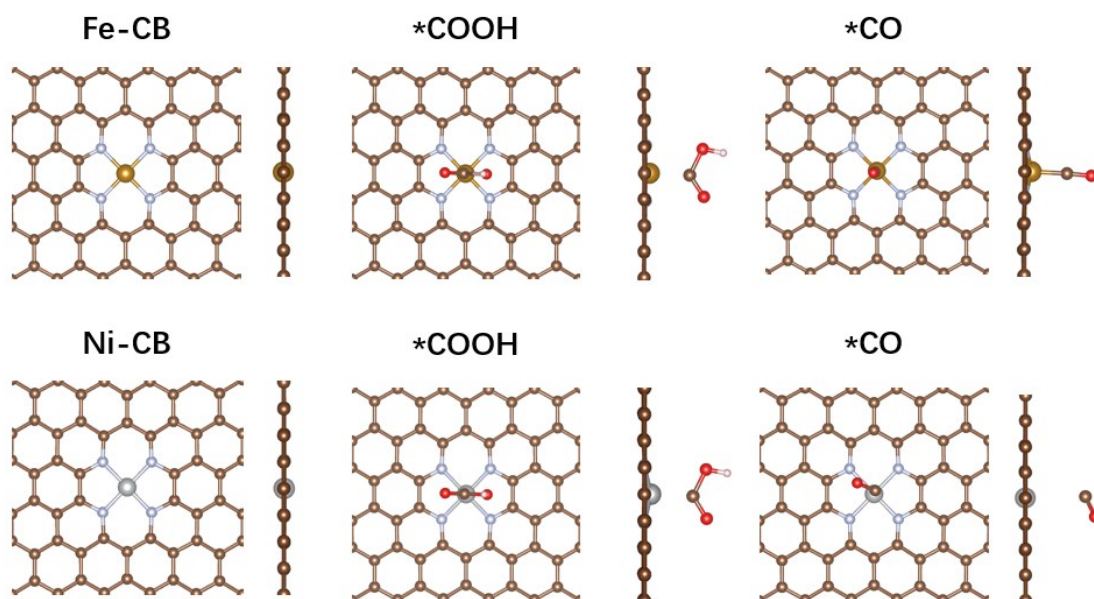


Fig. S15 Optimized structures of the intermediates on Fe-CB (up) and Ni-CB (down) catalysts.

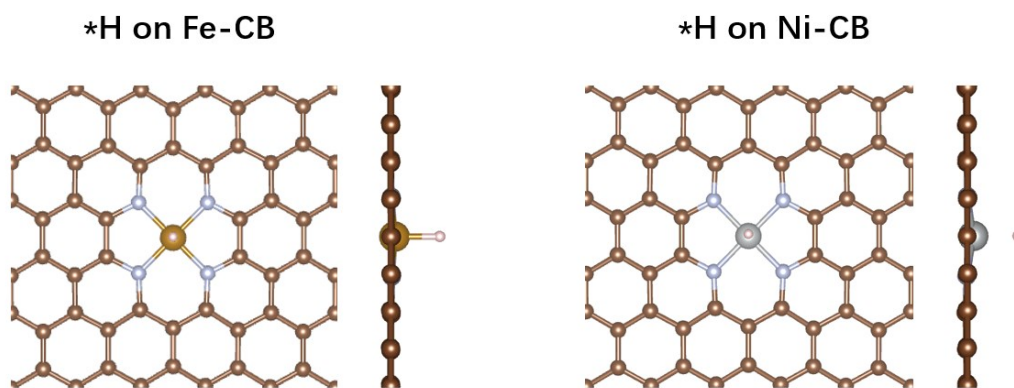


Fig. S16 Optimized structures of the *H intermediates on Fe-CB (left) and Ni-CB (right) catalysts.

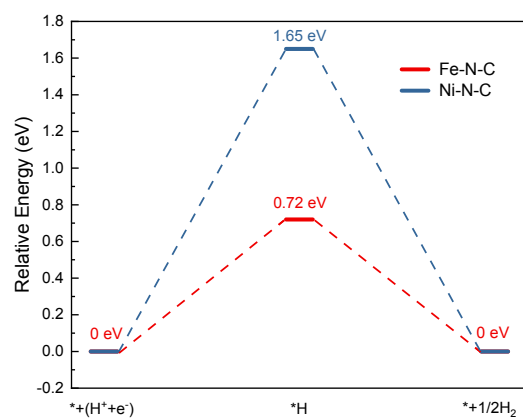


Fig. S17 Free energy diagram for the H_2 evolution at $E = 0$ V vs. RHE on Fe-N-C and Ni-N-C.

Table S1 Faradaic efficiency comparison of Fe-CB with reported Fe-N-C electrocatalysts

<i>Catalyst</i>	<i>Precursors</i>	<i>Product</i>	<i>FE_{CO} (%)</i>	<i>Over Potential (V)</i>	<i>Ref</i>
<i>Fe-CB</i>	TPPFeCl/CB	CO/H ₂	97	0.35	This Work
<i>Fe³⁺-N-C</i>	ZIF-8(Fe)	CO/H ₂	~95	0.35	16
<i>Fe-SAs/N-C</i>	ZIF-8(Fe)	CO/H ₂	~99	0.34	17
<i>Fe-N-C</i>	ZIF-8(Fe)	CO/H ₂	~93	0.49	18
<i>Fe₁-N-C</i>	Fe-PCN-222	CO/H ₂	~86	0.39	19
<i>Fe-N-C</i>	Fe ³⁺ /o-Phenylenediamine	CO/H ₂	~85	0.34	20
<i>Fe-N-C</i>	Fe ³⁺ /Polyaniline/Ketjen600EC	CO/H ₂	~75	0.44	21
<i>Fe-N-C</i>	Fe ³⁺ /Urea/CB	CO/H ₂	87	0.39	22
<i>Fe-N-C (3%)</i>	Fe ³⁺ /Urea-formaldehyde resin	CO/H ₂	74	0.49	23
<i>Fe-SA-900</i>	Fe ³⁺ /Dicyandiamide/Glucose	CO/H ₂	~90	0.47	24

Table S2 Catalytic performance comparison with reported heterogeneous noble-metal free CO₂ to CO conversion systems

<i>Catalytic System</i>	<i>Solvent</i>	<i>Light</i>	<i>Sacrificial Agent</i>	<i>Products</i>	<i>Yield of CO (mmol g_{cat}⁻¹ h⁻¹)/Time (h)</i>	<i>TON (CO)/Time (h)</i>	<i>Selectivity_{CO}(%)</i>	<i>Ref</i>
<i>Fe-CB+CdS</i>	0.5 M KHCO ₃ (aq)	AM 1.5G	TEOA	CO/H ₂	111/8	1220/ 8h	85	This Work
<i>polymeric cobalt phthalocyanine/mesoporous CN</i>	Acetonitrile	AM 1.5G	TEOA	CO/H ₂	1/48	84/48 h	85	25
<i>Co²⁺@C₃N₄</i>	Acetonitrile	λ>350 nm	TEOA	CO/H ₂	~	100/2 h	< 80	26
<i>MOF-525-Co</i>	Acetonitrile	λ>400 nm	TEOA	CO/CH ₄	1.2/6	1.19/6 h	84.5	27
<i>Co₁-G/CN</i>	Acetonitrile/Water	λ>420 nm	TEOA	CO/H ₂	0.16/6	25/6 h	30.3	28
<i>2D CN-COF</i>	Water	300 W Xe lamp	Water	CO/CH ₄	0.042/4	~	75	29
<i>O/La-CN</i>	Acetonitrile	300 W Xe lamp	TEOA	CO/CH ₄ /H ₂	0.46/5	~	80	30
<i>CTF-BP</i>	Acetonitrile/Water	λ>420 nm	TEOA	CO/CH ₄	0.046/10	~	37	31
<i>LZS</i>	Water	300 W Xe lamp	Water	CO	0.76/6	~	~	32

Table S3 Gibbs free energies (G) calculation at 298 K and 1 atm

	E_{DFT} (eV)	E_{ZPE} (eV)	$\int_0^{298} C_V dT$ (eV)	$-T\Delta S$ (eV)	G (eV)
H ₂	-6.769	0.265	-	-0.280	-6.784
CO ₂	-22.956	0.268	-	-0.724	-23.412
CO	-14.778	0.132	-	-0.614	-15.260
H ₂ O [†]	-14.223	0.567	-	-0.566	-14.222
Ni-N-C	-646.624	-	-	-	-646.624
*COOH	-671.671	0.623	0.105	-0.214	-671.157
*CO	-661.427	0.148	0.060	-0.137	-661.279
*H	-648.526	0.168	0.012	-0.017	-648.363
Fe-N-C	-648.848	-	-	-	-648.848
*COOH	-674.915	0.615	0.086	-0.175	-674.587
*CO	-665.158	0.221	0.062	-0.133	-665.008
*H	-651.709	0.190	0.005	-0.007	-651.520

[†] H₂O was calculated under 0.035 atm.

Reference:

- 1 J.-H. Guo and W.-Y. Sun, *Appl. Catal. B*, 2020, **275**, 119154.
- 2 X. F. Xie, X. Y. Dao, F. Guo, X. Y. Zhang, F. M. Wang and W. Y. Sun, *ChemistrySelect*, 2020, **5**, 4001-4007.
- 3 Q. Li, B. Guo, J. Yu, J. Ran, B. Zhang, H. Yan and J. R. Gong, *J. Am. Chem. Soc.*, 2011, **133**, 10878-10884.
- 4 Q. Jia, N. Ramaswamy, H. Hafiz, U. Tylus, K. Strickland, G. Wu, B. Barbiellini, A. Bansil, E. F. Holby, P. Zelenay and S. Mukerjee, *ACS Nano*, 2015, **9**, 12496-12505.
- 5 R. Zhang, L. Jiao, W. Yang, G. Wan and H.-L. Jiang, *J. Mater. Chem. A*, 2019, **7**, 26371-26377.
- 6 L. Jiao, G. Wan, R. Zhang, H. Zhou, S.-H. Yu and H.-L. Jiang, *Angew. Chem. Int. Ed.*, 2018, **57**, 8525-8529.
- 7 G. Kresse and J. Furthmuller, *Phys Rev B*, 1996, **54**, 11169-11186.
- 8 G. Kresse and D. Joubert, *Phys Rev B*, 1999, **59**, 1758-1775.
- 9 J. P. Perdew, K. Burke and M. Ernzerhof, *Phys. Rev. Lett.*, 1996, **77**, 3865-3868.
- 10 C. T. Dinh, T. Burdyny, M. G. Kibria, A. Seifitokaldani, C. M. Gabardo, F. P. Garcia de Arquer, A. Kiani, J. P. Edwards, P. De Luna, O. S. Bushuyev, C. Zou, R. Quintero-Bermudez, Y. Pang, D. Sinton and E. H. Sargent, *Science*, 2018, **360**, 783-787.
- 11 A. A. Peterson, F. Abild-Pedersen, F. Studt, J. Rossmeisl and J. K. Nørskov, *Energy Environ. Sci.*, 2010, **3**, 1311-1315.
- 12 J. K. Nørskov, J. Rossmeisl, A. Logadottir, L. Lindqvist, J. R. Kitchin, T. Bligaard and H. Jonsson, *J Phys Chem B*, 2004, **108**, 17886-17892.
- 13 R. Dronskowski and P. E. Bloechl, *J. Phys. Chem.*, 1993, **97**, 8617-8624.
- 14 V. L. Deringer, A. L. Tchougréeff and R. Dronskowski, *J. Phys. Chem. A*, 2011, **115**, 5461-5466.
- 15 S. Maintz, V. L. Deringer, A. L. Tchougréeff and R. Dronskowski, *J. Comput. Chem.*, 2016, **37**, 1030-1035.
- 16 J. Gu, C.-S. Hsu, L. Bai, H. M. Chen and X. Hu, *Science*, 2019, **364**, 1091-1094.

- 17 F. Quan, G. Zhan, H. Shang, Y. Huang, F. Jia, L. Zhang and Z. Ai, *Green Chemistry*, 2019, **21**, 3256-3262.
- 18 F. Pan, H. Zhang, K. Liu, D. Cullen, K. More, M. Wang, Z. Feng, G. Wang, G. Wu and Y. Li, *ACS Catal.*, 2018, **8**, 3116-3122.
- 19 L. Jiao, W. Yang, G. Wan, R. Zhang, X. Zheng, H. Zhou, S. H. Yu and H. L. Jiang, *Angew Chem Int Ed Engl*, 2020, **59**, 20589-20595.
- 20 X.-M. Hu, H. H. Hval, E. T. Bjerglund, K. J. Dalgaard, M. R. Madsen, M.-M. Pohl, E. Welter, P. Lamagni, K. B. Buhl, M. Bremholm, M. Beller, S. U. Pedersen, T. Skrydstrup and K. Daasbjerg, *ACS Catal.*, 2018, **8**, 6255-6264.
- 21 T. Möller, W. Ju, A. Bagger, X. Wang, F. Luo, T. Ngo Thanh, A. S. Varela, J. Rossmeisl and P. Strasser, *Energy Environ. Sci.*, 2019, **12**, 640-647.
- 22 L. Takele Menisa, P. Cheng, C. Long, X. Qiu, Y. Zheng, J. Han, Y. Zhang, Y. Gao and Z. Tang, *Nanoscale*, 2020, **12**, 16617-16626.
- 23 J. Zhao, J. Deng, J. Han, S. Imhanria, K. Chen and W. Wang, *Chemical Engineering Journal*, 2020, **389**.
- 24 C. Xu, A. Vasileff, D. Wang, B. Jin, Y. Zheng and S.-Z. Qiao, *Nanoscale Horizons*, 2019, **4**, 1411-1415.
- 25 S. Roy and E. Reisner, *Angew. Chem. Int. Ed.*, 2019, **58**, 12180-12184.
- 26 P. Huang, J. Huang, S. A. Pantovich, A. D. Carl, T. G. Fenton, C. A. Caputo, R. L. Grimm, A. I. Frenkel and G. Li, *J. Am. Chem. Soc.*, 2018, **140**, 16042-16047.
- 27 H. Zhang, J. Wei, J. Dong, G. Liu, L. Shi, P. An, G. Zhao, J. Kong, X. Wang, X. Meng, J. Zhang and J. Ye, *Angew. Chem. Int. Ed.*, 2016, **55**, 14310-14314.
- 28 C. Gao, S. Chen, Y. Wang, J. Wang, X. Zheng, J. Zhu, L. Song, W. Zhang and Y. Xiong, *Adv. Mater.*, 2018, **30**, e1704624.
- 29 X. Song, Y. Wu, X. Zhang, X. Li, Z. Zhu, C. Ma, Y. Yan, P. Huo and G. Yang, *Chem. Eng. J.*, 2020, DOI: 10.1016/j.cej.2020.127292.
- 30 P. Chen, B. Lei, X. Dong, H. Wang, J. Sheng, W. Cui, J. Li, Y. Sun, Z. Wang and F. Dong, *ACS Nano*, 2020, DOI: 10.1021/acsnano.0c07083.
- 31 J. Li, P. Liu, H. Huang, Y. Li, Y. Tang, D. Mei and C. Zhong, *Acs Sustain Chem Eng*, 2020, **8**, 5175-5183.

32 L. Wang, D. W. Bahnemann, L. Bian, G. Dong, J. Zhao and C. Wang, *Angew. Chem. Int. Ed.*, 2019, **58**, 8103-8108.